Research Square

Preprints are preliminary reports that have not undergone peer review.
They should not be considered conclusive, used to inform clinical practice,
or referenced by the media as validated information.

# Global warming increases lightning activity over Brazil regardless of the trend in cloud ice content simulated by a GCM

**Caio Lucas Texeira Ferraz De Oliveira**

caio.l.t.f.oliveira@gmail.com

National Institute for Space Research: Instituto Nacional de Pesquisas Espaciais
https://orcid.org/0000-0002-1314-7576

**Kleber Pinheiro Naccarato**

National Institute for Space Research: Instituto Nacional de Pesquisas Espaciais

**Research Article**

**Keywords:** Lightning, Climate Change, Global Circulation Models

**Posted Date:** July 27th, 2026

**DOI:** https://doi.org/10.21203/rs.3.rs-10176118/v1

**License:** This work is licensed under a Creative Commons Attribution 4.0 International License.
Read Full License

# Abstract

Global warming may modify lightning activity, although projections remain uncertain due to the diversity of parameterizations that emphasize different physical controls on atmospheric electrification, including atmospheric instability, cloud-top height, and ice content. This study projects changes in lightning density over Brazil by the end of the century using observations from the World Wide Lightning Location Network, ERA5 reanalysis, and climate projections from the EC-EARTH3-VEG Global Climate Model (GCM) under intermediate- and high-emission scenarios. Atmospheric predictors physically related to storm electrification were selected based on spatial correlations, skill in reproducing the seasonal cycle of lightning, statistical significance, and performance in simulating observed lightning in multivariate linear regression models. Convective available potential energy, total cloud ice content, convective precipitation rate, and mean sea level pressure emerged as the main controls. Two models were developed: one explicitly including cloud ice content and another using convective precipitation rate and mixed-phase depth as indicators of realized convection and ice formation potential. Both models reproduce the observed spatial and seasonal variability and project a spatially widespread increase in lightning density over Brazil in 2071–2100, with thermal sensitivity ranging from 8 to 11.5% $K^{-1}$ and absolute changes from 14 to 51%, depending on the predictors and scenario. The Brazilian Amazon shows the largest increases, reaching 9–24% $K^{-1}$, thereby increasing the risk of lightning-ignited fires in a forest that is becoming progressively more susceptible to fire.


# 1. Introduction

The future of lightning remains one of the major sources of uncertainty in climate science under global warming. This uncertainty arises from the complex processes involved in cloud electrification, which are best described by the noninductive charging theory (see the Supplementary Introduction for further details on cloud electrification), and is amplified by fundamental inconsistencies among competing lightning parameterizations in atmospheric models. Most studies project an increase in lightning activity under global warming (Price and Rind 1990; Price and Rind 1994; Michalon et al. 1999; Del Genio et al. 2007; Krause et al. 2014; Romps et al. 2014; Chakraborty et al. 2021; Chen et al. 2021; Pérez-Invernón et al. 2023), generally using proxies such as cloud-top height (CTH), convective available potential energy (CAPE), or other thermodynamic variables. However, other studies indicate a possible decrease in tropical regions when lightning is parameterized using cloud ice flux (Finney et al. 2014; Finney et al. 2018).

Projections based on cloud ice are particularly relevant because ice cloud content is directly involved in the physical process of electrification. These projections are generally derived from Global Circulation Models (GCMs), which reduce computational demands compared with high-resolution models. Under warming scenarios, GCMs often simulate a reduction in cloud ice content, which may lead to projections of decreased electrical activity, especially in tropical regions (Finney et al. 2018). A limited number of high-resolution convection-permitting studies have also been conducted for specific regions, indicating heterogeneous projections for lightning and graupel (Finney et al. 2020; Kahraman et al. 2022).

Among these studies, Multiple Linear Regression (MLR) and logistic regression have been used as more flexible models, in which the combination of predictors is selected a posteriori based on agreement with observations and the physical consistency of the explanatory variables (dos Santos et al. 2017; Chakraborty et al. 2021; Chen et al. 2021; Naccarato et al. 2022; Whaley et al. 2024). This differs from process-based parameterizations, in which the functional form is prescribed a priori and subsequently calibrated against observations (Price and Rind 1990, 1994; Michalon et al. 1999; Del Genio et al. 2007; Krause et al. 2014; Romps et al. 2014; Finney et al. 2014; 2018; 2020; Kahraman et al. 2022; Pérez-Invernón et al. 2023). MLR-based approaches project an increase in lightning activity, although they do not include cloud ice as a predictor, including in tropical regions (dos Santos et al. 2017; Chakraborty et al. 2021; Naccarato et al. 2022). In turn, Whaley et al. (2024) projected a decrease in tropical lightning activity associated with an increase in the Lifting Condensation Level (LCL), driven by reduced relative humidity and, therefore, greater atmospheric stability in the future. This effect offsets the increase in CAPE and occurs independently of cloud-ice-based parameterizations.

These empirical regression-based approaches remain limited by their dependence on long, bias-corrected time series and by important statistical assumptions, particularly the independence of observations. Temporal dependence in lightning data can violate these assumptions, leading to biased estimates of standard errors and, consequently, unreliable p-values for regression coefficients. This weakens statistical inference and limits the robustness of variable selection procedures based exclusively on regression coefficients (Wilks, 2011, pp. 245–250). In addition, empirical models trained under the present climate require predictors that represent relative thermodynamic and dynamic conditions rather than absolute magnitudes, such as specific humidity, cloud liquid water content, and temperature. This is because increases in these variables under global warming, largely associated with the Clausius-Clapeyron relationship, do not necessarily imply proportional increases in convective intensity or lightning activity (Molina et al. 2021; Beucler et al. 2024).

This debate has also been hampered by inconsistencies and biases in observational lightning datasets. Satellite records from the Lightning Imaging Sensor (LIS) and the Optical Transient Detector (OTD) are limited by low temporal resolution and uncorrected detection efficiency, particularly over South America, where the South Atlantic Magnetic Anomaly (SAMA) contaminates optical observations (Cecil et al. 2014; Chakraborty et al. 2021). In turn, studies based on ground-based networks have been constrained by geographically sparse and heterogeneous datasets, which have hindered robust analyses of climate-scale trends (Koshak et al. 2015; dos Santos et al. 2017; Paulucci et al. 2019; Bieniek et al. 2020; Holzworth et al. 2021; Amador and Arce-Fernández 2022; Naccarato et al. 2022).

Understanding the future evolution of lightning is important because of its role in atmospheric chemistry, forest ecological balance, impacts on civil infrastructure, risks to human life, and potential feedbacks on global warming. This key atmospheric phenomenon causes fatalities and damages critical urban infrastructure, including power grids and communication systems, especially in poorer regions (Holle 2016). In addition, lightning produces nitrogen oxides, which enhance tropospheric ozone (Jiang and Liao 2013) and contribute to global warming (Sinha and Toumi 1997). It may also ignite wildfires in the

Amazon and Atlantic Forest, where deforestation has increased the vulnerability of these tropical moist forests to fire (Cochrane and Laurance 2008; Pivello 2011).

In addition, lightning also contributes to the mortality of large trees (Slik et al. 2013; Johnson et al. 2016), disproportionately affecting these biomass-rich individuals that structure tropical forests. Although large trees account for less than 3% of stems, they store a substantial fraction of forest carbon, making them key regulators of the global carbon cycle (Slik et al. 2013). Lightning is among the main natural drivers of mortality for these trees, accounting for up to 17% of the deaths of giant Amazonian trees, with cascading effects on forest structure and long-term carbon storage (Johnson et al. 2016). Beyond mortality, lightning also influences forest composition (Gora et al. 2020). These impacts reinforce recent evidence that the Amazon carbon sink is weakening due to increasing tree mortality (Brienen et al. 2015), indicating that more frequent lightning under a warming climate may accelerate the decline of one of the planet's largest terrestrial carbon reservoirs and sinks.

These concerns are compounded by the scarcity of lightning projections for South America, with only two available studies, focused on the Brazilian states of São Paulo (dos Santos et al. 2017) and Santa Catarina (Naccarato et al. 2022). Therefore, this study investigates how future changes in atmospheric thermodynamics and cloud-ice microphysics may affect lightning activity in Brazil throughout the twenty-first century. Using physically based proxies derived from atmospheric variables available in both observational datasets and global climate models, we quantify how projected changes in convective energy and cloud-ice content influence lightning density. Brazil provides a unique natural laboratory because it encompasses tropical monsoon (Gan et al. 2004), equatorial (Rao and Hada 1990; Marengo et al. 2024), and subtropical (Ribeiro and Seluchi 2019) climate regimes, allowing the results to be interpreted within a broader climatic context. Specifically, we assess the atmospheric controls on the spatial variability of lightning, their evolution under global warming, projected changes in lightning density, and whether changes in cloud-ice content associated with thermodynamic changes may modify the relationship between atmospheric instability and electrical activity, either amplifying or offsetting the effects of increasing CAPE.

# 2. Materials and Methods

# 2.1. Data

# 2.1.1. Atmospheric data

Observational atmospheric data were obtained from the ERA5 reanalysis, produced by the European Centre for Medium-Range Weather Forecasts. This reanalysis is based on a global numerical weather prediction system that assimilates a wide variety of observations. ERA5 provides hourly data with a horizontal resolution of approximately 31 km and 137 pressure levels extending up to 1 Pa. These characteristics make ERA5 a benchmark dataset for evaluating climate model performance and

providing boundary conditions in long-term climate studies. Both single-level and pressure-level data were utilized (Hersbach et al. 2023a, b).

Future climate data were obtained from the Coupled Model Intercomparison Project Phase 6 (CMIP6) (O'Neill et al. 2016) which provides coordinated climate projections for use in IPCC assessments. In this study, we utilized the EC-Earth3-Veg Earth system model (Döscher et al. 2022), which employs the Integrated Forecasting System (IFS), also used in ERA5. This ensures physical consistency between the reanalysis and the simulations. EC-Earth3-Veg includes support for the Shared Socioeconomic Pathways (SSPs); in this study, the SSP245 and SSP585 scenarios were selected. Bias assessments indicate that EC-Earth3-Veg tends to underestimate precipitation by up to -70% in northern Brazil during summer and underestimate or overestimate it by up to + 100% in the Northeast, due to persistent double ITCZ patterns, a common feature in GCMs. The model also exhibits seasonal cold and warm biases of up to ± 5°C. However, its biases have a smaller spatial extent than those of most CMIP6 models, and the model ranks among the top performers in simulating Amazon precipitation and La Plata Basin temperature (Reboita et al. 2024). Monthly mean data from both datasets were utilized.

### 2.1.2. Lightning data

Lightning observations were obtained from the World Wide Lightning Location Network (WWLLN), which operates in the very-low-frequency (VLF) range, specifically within the 6 to 22 kHz intermediate band (Dowden et al. 2002). The hourly Relative Detection Efficiency (RDE) maps published by Hutchins et al. (2012) were spatially and temporally averaged to produce monthly RDE time series for each grid cell within the study domain. WWLLN was selected because it provides global coverage and higher temporal resolution than the commonly used LIS/OTD datasets.

## 2.2. Methods

### 2.2.1. Data processing and normalization

All datasets were harmonized to a common monthly temporal resolution and mapped onto a 1° × 1° land-only grid over Brazil. WWLLN lightning records were quality-controlled, filtered to the Brazilian land domain, aggregated by grid cell and month, and converted to lightning density by dividing monthly stroke counts by the land area of each grid cell. The resulting densities were corrected using monthly RDE fields. The analysis period spans 2013–2025, selected to avoid the rapid increase in WWLLN detection efficiency before 2013 (Hutchins et al. 2012), with 2013–2022 used for model training and 2023–2025 for validation. ERA5 pressure-level and single-level variables were aggregated to the same grid using area-weighted mapping based on geometric overlap with the land fraction of each target cell. EC-Earth3-Veg predictor fields were processed using the same grid structure and variables to ensure consistency between reanalysis-based model training and future projections. Future projections were derived from the Shared Socioeconomic Pathways SSP245, an intermediate forcing scenario, and SSP585, a high-emission scenario (O'Neill et al. 2016), extending up to 2100. Further details on land masking, area calculation, spatial joins, and area-weighted remapping are provided in the Supplementary Methods.

## 2.2.2. Atmospheric proxies' selection

The initial set of atmospheric variables was defined to evaluate both emergent convective and microphysical properties as well as climate-relative and climate-invariant measures, following recent methodological recommendations for empirical climate models. Consequently, absolute thermodynamic baseline atmospheric state variables, such as specific humidity, air temperature, and sea surface temperature, were excluded from the analysis, as recommended by Beucler et al. (2024). Instead, selected absolute variables, including convective precipitation rate, total column ice content, vertical velocity, CAPE, and related fields, were retained because they represent emergent properties of convective and microphysical processes, rather than thermodynamic states indirectly related to lightning. These variables were tested alongside relative measures, such as plume buoyancy and mid-level moisture deficit, to identify physically consistent proxies capable of capturing electrification efficiency and intensity, while simultaneously reducing sensitivity to uniform thermodynamic shifts associated with global warming. The final set of predictors utilized in the regression models was selected empirically, based on individual spatial correlation, individual statistical significance, and overall explained variance during the testing phase. Supplementary Table 1 lists the 14 variables utilized in the subsequent analysis. A detailed description of the calculation of the derived variables is provided in the Supplementary Methods.

The initial selection of ERA5 atmospheric proxies was designed to provide an independent inferential basis for variable choice, avoiding reliance on regression slope p-values, which can be biased due to temporal dependence in the data. For each candidate ERA5 variable, correlations between lightning density and the values at each grid cell were calculated using both Pearson and Spearman coefficients. Variables were ranked using a composite score that combined the mean absolute spatial correlation, the fraction of statistically significant grid cells, the spatial consistency of the correlation pattern, and the ability to reproduce the climatological seasonal cycle of lightning. Variables with low final scores were excluded from subsequent modeling, and the remaining predictors were utilized to define a hierarchy of physically interpretable atmospheric controls. Full details of the scoring procedure are presented in the Supplementary Methods.

MLR models were then evaluated using combinations of the top-ranked predictors, prioritizing variables that represented distinct physical processes related to convective instability, realized convecção, cloud microphysics, and large-scale dynamic modulation. Model performance was assessed at both the grid-cell and domain scales. Cell-level diagnostics, i.e., an MLR for each cell, included $R^2$ in the training period, RMSE and bias in the validation period, F-test significance, and Variance Inflation Factors (VIF) to assess multicollinearity. Domain-scale performance was evaluated using domain-averaged time series of the atmospheric variables by fitting a single MLR for the entire Brazilian domain, and included $R^2$, RMSE, bias, and Pearson correlation during validation. Predictor combinations were progressively expanded from the top-ranked variables, and interaction terms were tested to evaluate coupled physical effects. Full details of the performance evaluation procedure are presented in the Supplementary Methods.

Finally, two models were selected based on their overall performance and physical interpretability. One model explicitly included cloud ice content, whereas the other excluded this variable, incorporating proxies that mimic its effect. This approach was adopted due to the known uncertainty and potential bias in the simulation of cloud ice by GCMs, allowing for a more robust assessment of lightning projections.

### 2.2.3. Bias correction and trend analysis

For bias correction, a distribution-based scaling method was applied, adapted from Feddersen et al. (1999) and Wood et al. (2002), and previously used in lightning projections (dos Santos et al. 2017). This approach adjusts the simulated data by aligning its mean and standard deviation with those of the reference dataset.

For each atmospheric variable and grid cell, bias-correction parameters were calculated over a common reference period by comparing the EC-Earth simulations with ERA5. The corrected values were then obtained by scaling the simulated anomalies relative to the model climatology and rescaling them using the observed climatology. This correction was applied independently to each predictor and grid cell, ensuring that both the central tendency and the variability of the simulated data are consistent with the observational reference.

Supplementary Fig. 4 shows the climatological relative bias of EC-Earth3-Veg relative to ERA5 for the variables selected as predictors, based on the results and discussion presented in the following sections. Supplementary Fig. 5 shows the bias-corrected climatology and the residual bias for the independent validation period, 2023–2025.

For the trend analysis of atmospheric variables and projected lightning density, the non-parametric Mann-Kendall test and Sen's slope estimator were applied. To quantify the thermodynamic sensitivity of lightning activity to warming, we computed a fractional change metric in % $K^{-1}$, following Romps (2019), using global mean near-surface temperature from EC-Earth3-Veg.

## 3. Results and discussions

## 3.1. Atmospheric variable initial selection

The initial screening identified variables representing atmospheric instability, effectively realized convection manifested in precipitation, and microphysics as the primary control factors over lightning activity (Table 1). CAPE ranked first, exhibiting positive Pearson and Spearman spatial correlations with lightning density across the entire domain (Supplementary Figs. 1n and 2n), as well as strong agreement with its mean annual cycle (Supplementary Fig. 3n). ICE ranked second, also displaying widespread positive spatial correlations and a coherent seasonal cycle relative to lightning density (Supplementary Figs. 1d, 2d, and 3d). CPR and ThetaE followed, with predominantly positive correlations across most of Brazil and consistent behavior in the annual cycle (Supplementary Figs. 1b, 2b, 1j, 2j, 3b, and 3i). Overall,

the top-ranked predictors represent energy availability, active convective intensity, given by the capacity to generate convective precipitation, and mixed-phase microphysics, whereas lower-ranked variables provide more regional or secondary information.

Table 1
Final ranking score of atmospheric variables.

| rank | Variable | Score Pearson | Score Spearman | Score Annual Cycle | Score Final |
|---|---|---|---|---|---|
| 1 | CAPE | 0.8123 | 0.8222 | 0.7929 | 0.8124 |
| 2 | ICE | 0.7808 | 0.8102 | 0.7422 | 0.7848 |
| 3 | CPR | 0.6946 | 0.6913 | 0.6638 | 0.6871 |
| 4 | ThetaE | 0.6549 | 0.6502 | 0.6793 | 0.6579 |
| 5 | Omega500 | 0.6456 | 0.6763 | 0.6044 | 0.6496 |
| 6 | MHD | 0.6251 | 0.6228 | 0.6266 | 0.6245 |
| 7 | CSP | 0.5786 | 0.5852 | 0.5771 | 0.5809 |
| 8 | MSLP | 0.5862 | 0.5672 | 0.586 | 0.5786 |
| 9 | CRH | 0.5921 | 0.5813 | 0.5061 | 0.5706 |
| 10 | EEF | 0.6152 | 0.595 | 0.3707 | 0.5582 |
| 11 | MPD | 0.4276 | 0.4119 | 0.2893 | 0.3937 |
| 12 | PB | 0.4022 | 0.3815 | 0.2343 | 0.3603 |
| 13 | CINE | 0.0995 | 0.0633 | 0.0525 | 0.0756 |
| 14 | WS | 0.0948 | 0.0604 | 0 | 0.0621 |

The spatial correlations further suggest three regimes for the relationship between lightning and the atmospheric environment (Supplementary Figs. 1 and 2). The first encompasses central Brazil, including the Central-West, Southeast, and southern Amazon, where lightning density shows a strong and consistent correlation with CAPE, CRH, MHD, Omega500, and ICE. This pattern is consistent with a monsoon-influenced tropical continental regime, in which seasonal low-level heating, moisture accumulation, and atmospheric instability favor deep convection (Gan et al. 2004). In this region, therefore, electrical activity is closely linked to thermodynamic forcing and convective depth.

The second regime occurs in the far northern Amazon, including Amapá and the equatorial band. In this region, CPR, CRH, CINE, MHD, and CSP exhibit weak, neutral, or even opposite correlations with lightning density, frequently with low statistical significance. This pattern likely reflects a persistently warm and humid equatorial environment, characterized by frequent convection and weak seasonal contrast between favorable and unfavorable convective states. Such behavior is consistent with the rainfall climatology of northern Brazil, which is governed by the meridional displacement of the Atlantic ITCZ

and the annual migration of Amazonian deep convection (Rao and Hada 1990; Marengo et al. 2024). Under these conditions, classical instability predictors lose discriminatory power, as the environment frequently remains close to convective thresholds. The difficulty of climate models in representing the ITCZ, combined with larger precipitation biases over northern Brazil (Reboita et al. 2024), may further weaken these relationships.

The third regime corresponds to southern Brazil, where weaker correlations of several pre-convective thermodynamic variables indicate a stronger control exerted by ongoing convective intensity and synoptic forcing. Fronts and troughs frequently initiate or sustain storms in this region (Ribeiro and Seluchi 2019), reducing the diagnostic value of CINE, CSP, EEF, and even CAPE. In contrast, variables associated with active convection, especially ICE, CPR, and Omega500, maintain greater relevance. Across the three regimes, ICE remains consistently important, indicating that electrification is systematically linked to mixed-phase microphysics, despite regional differences in triggering mechanisms and convective organization. Overall, the final ranking reflects the combined roles of instability, convective intensity, and cloud ice. Variables with final scores below approximately 0.4, namely PB, CINE, and WS, were excluded from subsequent analyses.

## 3.2. Performance-based selection of RLM models

Following the initial screening of predictors, model performance was evaluated based on the ability to explain the observed variance and simulation skill (Supplementary Table 2). First, models without interaction terms were tested. At the local scale, some predictor sets reduced the validation bias but also decreased the mean grid-cell $R^2$, indicating amplitude compression, with predictions closer to the climatological mean and a weaker representation of seasonality and extremes.

Among the thermodynamic predictors, CAPE consistently outperformed ThetaE. Although ThetaE remained informative, the ThetaE + ICE combination resulted in a lower domain-level $R^2$ than CAPE + ICE (0.80 vs. 0.85), despite exhibiting a lower mean grid-cell validation bias. Predictors related to instability or conditional stability, such as CSP and EEF, showed weaker performance, likely because linear models cannot fully represent threshold behavior, saturation, and state dependency. Their influence is better captured indirectly through realized convection and microphysics, represented by CPR and ICE. After all, if precipitation or cloud ice formation occurred, stability was overcome and CAPE was consumed.

A secondary formulation excluding ICE was tested to assess the sensitivity to potential GCM biases in ice-related variables. MPD and MHD captured part of the lightning activity information but exhibited lower performance than ICE. CAPE + MPD and CAPE + MHD produced mean grid-cell $R^2$ values of 0.40 and 0.43, respectively, compared to 0.47 for CAPE + ICE, with slightly lower domain-scale $R^2$ values of 0.82 and 0.81. The combination of MPD and MHD preserved the domain-scale $R^2$ of 0.81, but reduced stability, with only 62.3% of the grid cells satisfying VIF < 5. Thus, mixed-phase depth and mid-level humidity describe conditions favorable to ice formation and electrification, although they only partially substitute for ICE.

The CAPE + CPR+MPD model exhibited substantially better performance, equaling CAPE + ICE at the local scale (mean grid-cell $R^2$ = 0.47) and reaching a domain-scale $R^2$ of 0.84. This indicates that CPR represents realized convection from a conditionally unstable environment, while MPD approximates the vertical extent of the mixed-phase layer where charge separation occurs. Together, these variables recover much of the predictive information associated with ICE.

Adding ICE to the CAPE + CPR+MPD model increased the mean grid-cell $R^2$ from 0.47 to 0.50, with only a marginal increase in the domain-scale $R^2$ from 0.84 to 0.85. However, this combination substantially reduced model stability, as only 25% of the grid cells met the VIF < 5 criterion. This result supports the previous interpretation that CPR + MPD recover much of the information associated with ICE, due to the collinearity among these variables. The addition of MSLP produced a more substantial overall improvement: the mean grid-cell $R^2$ increased to 0.51, the RMSE decreased to 0.111, the validation bias decreased to -0.021, the domain-scale $R^2$ increased to 0.87, and 90% of the grid-cells maintained VIF < 5. These results indicate that, once convection and the mixed-phase structure are represented, MSLP provides additional dynamic modulation at the synoptic scale.

The CAPE + ICE+MSLP model also exhibited strong performance. Compared to CAPE + ICE, the inclusion of MSLP increased the mean grid-cell $R^2$ from 0.47 to 0.50 and the domain-scale $R^2$ from 0.85 to 0.90, with 100% of the grid cells satisfying the VIF < 5 criterion. The CAPE + CPR+MPD+MSLP model presented slightly better RMSE and validation bias at both the local and domain scales. These results support two physically consistent formulations: one based directly on ice content and another based on realized convection and the mixed-phase structure.

Compared to the CAPE×CPR proxy of Romps et al. (2014), which yielded a domain-scale $R^2$ of 0.72 and a mean grid-cell $R^2$ of 0.40, the CAPE + ICE+MSLP and CAPE + CPR+MPD+MSLP models achieved domain-scale $R^2$ values of 0.90 and 0.87, and mean grid-cell $R^2$ values of 0.50 and 0.51, respectively. The mean grid-cell spatial correlations between the observed and simulated climatological fields reached r = 0.95 for both final models, exceeding the value of r = 0.78 reported by Finney et al. (2018). The domain-scale correlations also reached r = 0.95 and r = 0.93, values higher than those reported by Chakraborty et al. (2021; r = 0.76) and dos Santos et al. (2017; r = 0.84).

Interaction terms did not improve model robustness. Although some improved the training fit, these gains did not persist during validation, and multicollinearity became severe. Overall, lightning density over Brazil is strongly controlled by the combined influence of thermodynamic, microphysical, and dynamic factors. The CAPE + ICE+MSLP model, hereafter referred to as Model 1, provides a physically direct formulation. The CAPE + CPR+MPD+MSLP model, hereafter referred to as Model 2, offers a robust alternative, exhibiting slightly better validation performance and lower dependence on ice-related variables, whose representation remains more uncertain in global climate simulations. However, the relative bias maps for CPR and ICE exhibited similar magnitudes (Supplementary Figs. 4 and 5). Together, these models provide a consistent framework for projecting future lightning activity, capturing both changes in ice content and variations in realized convection within conditionally unstable

environments, represented here by convective precipitation. Furthermore, they incorporate the influence of different synoptic regimes through the representation of pressure systems.

## 3.3. Projected trends in atmospheric predictors

Annual mean trends were computed to diagnose the future evolution of the selected atmospheric predictors and the associated convective environment (Fig. 1).

CAPE exhibits positive and statistically significant trends across Brazil, ranging from 3% to 9% per decade, with maxima in the Northeast, the northwestern Amazon, and localized areas in the Southeast and South (Fig. 1a). This result is consistent with the expected thermodynamic response to warming and with CAPE trends reported in previous studies (Romps et al. 2014; Romps 2019; Chakraborty et al. 2021; Chen et al. 2021). CSP also increases across the entire domain, primarily over central Brazil (Fig. 1h), while MSLP exhibits smaller positive trends, which are more intense over the South, Southeast, and Northeast of Brazil (Fig. 1g). Together, these variables indicate greater availability of convective potential energy within a more stable atmospheric mean state.

This configuration is consistent with the mechanism initially observed by Del Genio et al. (2007) and with the explicit convection models of Finney et al. (2020) and Kahraman et al. (2022), in which a more stable mean state reduces the overall frequency of convective events, while episodic dynamic forcing triggers the release of accumulated CAPE. The projected response therefore indicates less frequent, or similarly frequent (Rehbein et al., 2026), convectively active periods associated with greater intensity during these rare events. The central question is whether the more intense electrical activity of these rare events can compensate for the reduction in occurrence frequency and, if so, to what extent this compensation would be reflected in the overall domain average.

The regional responses of CPR reflect this balance (Fig. 1e). In northeastern Brazil, CPR decreases together with positive Omega500 trends, indicating mean subsidence and higher MSLP. In western and central Amazonia, Omega500 suggests an intensification of mean ascent, and CSP remains nearly neutral, although CPR still decreases. This reduction is likely driven by strong positive MHD trends (Fig. 1b), indicating drier midlevels and conditions less favorable for condensation, despite the intensification of upward motion. In southern Amazonia and central Brazil, the suppression of CPR is mainly associated with strong increases in CSP, which inhibit convective precipitation even where Omega500 indicates some intensification of ascent. Negative Omega500 trends may be associated with an increase in the intensity of these less frequent periods of instability, indicating that the greater magnitude of upward motions was sufficient to compensate for the reduced frequency of occurrence of these events.

ICE shows a similar spatial structure, with widespread reductions across tropical Brazil and increases in southern Brazil and parts of the far north (Fig. 1c), in broad agreement with the global pattern reported by Finney et al. (2018). Under warming conditions, a higher freezing level may reduce the efficiency of graupel and ice-particle formation. However, in the present results, the small positive MPD trends appear

insufficient to offset the strong increases in CAPE and CSP, which favor more intense updrafts during less frequent unstable periods. Therefore, the reduced frequency of these unstable periods appears to largely explain the negative trends observed in tropical ICE.

This interpretation is consistent with the pattern observed in southern Brazil, where stronger positive MPD trends coincide with larger increases in ICE, more modest increases in CSP, and nearly stable MHD values. Although the increase in MSLP and the positive Omega500 trends indicate a more stable mean environment, convection in this region remains strongly modulated by transient synoptic systems. The localized increases in CPR and ICE suggest that fronts and troughs continue to act as effective mechanisms for convective triggering. Once convection is initiated, the greater availability of CAPE favors more intense precipitation and enhanced ice production. In addition, more intense synoptic events may be followed by more persistent high-pressure conditions, helping to explain the increases in MSLP and Omega500. The near stability of MHD, in turn, indicates that midlevel moisture conditions remain sufficiently favorable for condensation and hydrometeor formation.

A distinct equatorial pattern emerges near 0° latitude, where CPR and ICE increase despite positive Omega500 and CSP trends. This apparent inconsistency can be interpreted within the same frequency-intensity framework: the mean state becomes more stable and subsident, while increasing CAPE provides a larger energy reservoir. When inhibition is overcome, likely in this region through variability associated with the ITCZ, storms become sufficiently intense to increase precipitation and ice production, offsetting the suppression imposed by the mean background state. This dynamic context also explains the weaker increase in MSLP compared with southern Brazil. In the South, transient baroclinic systems, such as cold fronts, are often followed by persistent anticyclonic conditions that raise mean surface pressure. ITCZ-related convection in the equatorial band lacks this persistent postfrontal high-pressure structure, so MSLP increases less.

## 3.4. Lightning projections

Projected lightning density for 2071–2100, expressed as fractional changes per kelvin of global warming, shows widespread increases across Brazil in both models. In Model 1 (CAPE + ICE+MSLP; Fig. 2), lightning density increases over most of the domain even with ICE included as a predictor, with localized reductions mainly restricted to Acre, in the far western Brazilian Amazon. The largest increases occur in northeastern Brazil, northwestern Brazilian Amazonia, including Roraima and northern Amazonas state, and along a continuous band extending across southern and southeastern Brazil. These spatial patterns are highly consistent between the SSP245 and SSP585 scenarios.

Model 2 (CAPE + CPR+MPD+MSLP; Fig. 3) produces a distinct yet complementary spatial response, with a strongly positive core over central and western Brazilian Amazonia and negative changes in parts of northeastern Brazil. Despite these differences, both models project localized increases in southern and southeastern Brazil, central Brazil, and the southern coast of northeastern Brazil. Positive trends in Amazonia and the reduction in Acre also persist, although the increases in central Amazonia are more

intense in Model 2 (12–25% $K^{-1}$), which excludes ICE and uses CPR and MPD to represent realized convection and the mixed-phase structure.

The cell-averaged metrics confirm a robust positive response at the domain scale. For 2071–2100, Model 1 projects fractional changes from 7.63% $K^{-1}$ under SSP245 to 8.14% $K^{-1}$ under SSP585, whereas Model 2 projects higher sensitivities, ranging from 10.62% $K^{-1}$ to 11.53% $K^{-1}$. In absolute terms, cell-averaged lightning density increases by 14.0% to 33.7% in Model 1 and by 20.1% to 50.9% in Model 2 under the SSP245 and SSP585 scenarios, respectively. Therefore, the increase in the intensity of electrical activity and in the severity of these rare events was sufficient to produce an increase in overall mean lightning density, compensating for the reduced frequency of occurrence.

These values are consistent with the 10% to 25% increase by the end of the century projected for India by Chakraborty et al. (2021), as well as with thermal sensitivities previously reported in studies without explicit ice-related predictors: 5% to 6% $K^{-1}$ in the global model based on CTH by Price and Rind (1994), 12 ± 5% $°C^{-1}$ in the CAPE × Precipitation model for the United States by Romps et al. (2014), and 8% to 16% $K^{-1}$ in CPM model simulations presented by Romps (2019).

These results differ from those obtained by Finney et al. (2018), who projected an approximately 15% global reduction in lightning flash rate by 2100 using an ice-flux-based parameterization, with the largest decrease occurring in the tropics. This difference may arise because monthly mean ice-related variables in each grid cell do not distinguish an actual reduction in ice content within individual storms from a reduction in the frequency of storms containing ice. In the IFLUX formulation, lightning flash rate scales linearly with upward cloud ice flux, which is computed from specific cloud ice water content and updraught mass flux. This multiplicative structure may make the projected lightning response particularly sensitive to reductions in mean cloud ice and mean updraught mass flux. By contrast, the present multiple linear regression framework includes ICE as one predictor together with CAPE and MSLP, allowing changes in cloud ice to be evaluated jointly with thermodynamic instability and large-scale dynamical controls. This formulation is less structurally constrained to translate decreases in mean ICE directly into decreases in lightning density and is therefore consistent with a positive lightning response when the effects of increasing CAPE outweigh reductions in mean ice content.

Two hypotheses are proposed here to explain the increase in lightning found alongside decreasing ICE. In the first, the projected reduction in ICE reflects an actual decrease in the amount of ice available within individual storms. In this case, the linear models used in this study may be capturing a compensatory mechanism, in which increasing CAPE partially mitigates the effects of this microphysical reduction. Under this scenario, higher CAPE values may intensify updrafts, increase collision velocities among hydrometeors, and strengthen charge-separation processes in convective events that are able to overcome inhibition, allowing lightning density to increase even under lower ice availability.

In addition, the expansion of the mixed-phase region, as shown in Fig. 1h, favors a greater probability of collisions among particles containing a quasi-liquid water layer on their surface, facilitating charge-transfer processes (Baker et al. 1987; Baker and Dash 1994). This result contrasts with previous

expectations regarding a decrease in charge-separation efficiency under a rising melting level, because the upper boundary of the mixed-phase region also rises, expanding the volume in which particle collisions can occur.

A second hypothesis is that the projected decrease in ICE in this and other GCM studies primarily reflects a reduction in the number of storms with substantial amounts of ice in the mixed-phase region, rather than a proportional decrease in ice content within each individual storm. In this case, the storms that do occur may still contain similar or even larger amounts of ice in the mixed-phase region and produce more intense electrification (increased severity).

This interpretation is consistent with a warmer climate characterized by lower relative humidity, higher cloud bases, and greater convective inhibition, in which fewer events can overcome the background atmospheric stability. For those events that do trigger convection, however, larger amounts of accumulated CAPE tend to be consumed, leading to greater hydrometeor condensate formation because of increased available specific humidity. This behavior has been observed in CPM studies conducted on other continents (Finney et al. 2020; Kahraman et al. 2022).

The mean reductions in convective mass flux and cloud cover reported by Finney et al. (2018) remain compatible with this interpretation, because grid-cell means combine information on storm occurrence, area, duration, and conditional intensity, thereby emphasizing reduced storm frequency relative to increased storm severity.

Determining which of these scenarios predominates requires decomposing ICE trends into frequency and severity components using data at a higher temporal resolution than the monthly data analyzed in this study.

A similar separation between frequency and severity was recently reported for Mesoscale Convective Systems (MCSs) in South America. Rehbein et al. (2026) found more robust evidence for increased MCS severity, expressed by higher maximum precipitation rates and larger precipitation volumes, than for widespread changes in the occurrence of these systems. This supports the interpretation that warming may favor more severe convective episodes, with larger amounts of condensed matter, even when the frequency response remains unchanged, as in their case, or even decreases. The projected reductions in tropical lightning reported by Whaley et al. (2024) may also reflect this dichotomy, since their logistic regression framework primarily captures changes in the probability of electrically active conditions. In contrast, the linear regressions used here are more sensitive to the magnitude of lightning density and therefore may represent intensification within less frequent events.

We also present the standardized regression coefficients of the two models (Supplementary Figs. 6 and 7). In Model 1, which explicitly includes ice content, CAPE shows a larger standardized contribution than in Model 2. This result suggests that, when ice availability is represented more directly, the variability in lightning density becomes more strongly associated with available convective energy. Physically, this combination is consistent with noninductive charging theory, in which electrification depends

simultaneously on the presence of frozen hydrometeors and on the intensity of updrafts that favor their transport and collisions. Thus, the greater relative importance of CAPE in Model 1 suggests that the thermodynamic processes associated with deep convection play a more evident role when ice availability is explicitly considered.

The spatial distribution of these coefficients reinforces the influence of regional climate regimes on electrification. In central Brazil, CAPE exhibits its largest predictive weights, confirming the thermodynamic control associated with the continental tropical regime. By contrast, in southern Brazil, the predictors of active convection, ICE in Model 1 and CPR in Model 2, become more relevant, highlighting the role of transient synoptic systems.

The slope coefficients for MSLP show positive signs along the coastal areas of southern and southeastern Brazil and, with smaller magnitude, in northeastern Brazil (Supplementary Figs. 6c and 7c). This result reinforces the previously suggested idea that the model captured a relationship in which periods of higher pressure in these regions are associated with the influence of more intense or more frequent low-pressure systems. Conversely, negative coefficients predominate in central-western, northern, and northwestern Brazil, indicating a more direct association between low pressures generated by daytime thermodynamic heating and the development of local convection.

However, the interpretation of the p-values associated with the multiple linear regression coefficients requires caution, as discussed in the Methods section. In this specific context, this limitation does not directly affect the interpretation of coefficient magnitudes. Additional caution is required because the linear formulations used here do not fully capture the nonlinear thresholds inherent to convective processes.

# 4. Conclusions

This study presents the first lightning projection for Brazil, a region that includes biomes central to the global carbon cycle and encompasses tropical, equatorial, and subtropical climates. Using WWLLN observations at high temporal resolution, which avoid the limitations of satellite optical records associated with the SAMA, together with ERA5 data and EC-Earth3-Veg projections, we assess the atmospheric controls on lightning under global warming within a reproducible GCM-based methodology.

To ensure robust predictor selection while accounting for the inferential limitations of multiple linear regression coefficients under temporal dependence, we used univariate spatial-correlation scores. CAPE, CPR, and ICE emerged as the strongest predictors of lightning density. The spatial variability of these correlations revealed three distinct regimes of association between lightning and the atmospheric environment, which were also reproduced by the spatial distribution of the regression slope coefficients. In central Brazil, a continental tropical regime links lightning primarily to thermodynamic control and convective depth. In the far northern Brazilian Amazon, a persistently humid equatorial regime reduces the contrast between conditions favorable and unfavorable to convection. In southern Brazil, a subtropical regime indicates a stronger dependence on active convection triggered by synoptic systems

than on preexisting local instability. Across all these regimes, ICE maintained a consistent correlation with lightning activity, indicating the central role of microphysical processes. Most strictly climate-invariant predictors showed weaker performance, except for MSLP, which was retained in the final models.

For 2071–2100, the models project a widespread increase in lightning density of approximately 8–11% $K^{-1}$, corresponding to absolute increases of 14–51%, depending on the scenario and predictor set. The largest increases occur over southern and southeastern Brazil, central Brazil, the southern coast of northeastern Brazil, and much of the Brazilian Amazon, whereas localized reductions are concentrated mainly in Acre state.

Despite differences in magnitude and spatial structure, both models indicate that the Brazilian Amazon will be one of the main hotspots of future intensification of lightning activity in Brazil. In Model 1, which explicitly includes ice content (ICE), the projected increases are generally modest across much of Amazonia but still reach approximately 9–19% $K^{-1}$ in the northwestern sector. In Model 2, which uses CPR and MPD to represent realized convection and the mixed-phase structure, the signal becomes stronger and more widespread, with extensive areas of central-western and northwestern Amazonia exceeding 12% $K^{-1}$ and local maxima approaching 24% $K^{-1}$. This convergence between models is important because it indicates that the increase in lightning activity over Amazonia is robust to how cloud ice is represented. In a biome increasingly affected by warming, humidity loss, deforestation, and fire susceptibility, this projected increase may amplify the risk of lightning-ignited wildfires.

These results help reconcile the decrease in mean cloud ice content with the increase in convective potential. Warming raises the freezing level and may reduce the total ice mass simulated by GCMs; however, this reduction does not appear sufficient to suppress the projected increases in lightning activity in our models. One possible explanation is that higher CAPE values intensify updrafts and increase collision rates among hydrometeors in convective events that can overcome inhibition, partially compensating for the lower mean ice availability. A complementary interpretation is that projected reductions in mean cloud ice content partly reflect decreases in storm frequency, without necessarily implying weaker individual storms. In this scenario, fewer storms may form in the future, while those that do develop may contain similar or even larger amounts of ice in the mixed-phase region and produce more intense electrification. Thus, future lightning activity across most of Brazil may be characterized by reduced storm frequency accompanied by greater electrical severity.

# Declarations


### Acknowledgments

We thank Dr. Robert Holzworth from the University of Washington, Seattle, USA, for providing the WWLLN lightning data. We also thank Dr. Ana Paula Paes dos Santos, Dr. Rosmeri Porfírio da Rocha, Dr. Chou Sin Chan, Dr. Lincoln Muniz Alves, and Dr. Cristiano Max Wrasse for their valuable suggestions on lightning projections.

**Funding**

We acknowledge financial scholarship support of CAPES (*Coordenação de Aperfeiçoamento de Pessoal de Nível Superior*), a Foundation of Ministry of Education, Brazil - Grant No. 88887.911747/2023-00 (Caio L. T. F. De Oliveira).

**Author contributions**

Caio L. T. F. De Oliveira and Kleber P. Naccarato conceived the study. Caio L. T. F. De Oliveira processed the data, performed the analyses, produced the figures, and wrote the first draft of the manuscript. Kleber P. Naccarato supervised the research and contributed to the interpretation of the results and revision of the manuscript. Both authors reviewed and approved the final manuscript.

**Availability of data and code**

ERA5 reanalysis data are available from the Copernicus Climate Data Store, including ERA5 hourly data on single levels (https://doi.org/10.24381/cds.f17050d7) and ERA5 hourly data on pressure levels (https://doi.org/10.24381/cds.6860a573). CMIP6 EC-Earth3-Veg model outputs are available from the Earth System Grid Federation for SSP245 (https://doi.org/10.22033/ESGF/CMIP6.488275) and SSP585 (https://doi.org/10.22033/ESGF/CMIP6.491476). The processed datasets generated in this study are available to reviewers through an anonymized peer-review repository [anonymous link]. The scripts used for data analysis and figure generation are also available to reviewers through the same link. Upon acceptance, the processed datasets and scripts will be archived publicly in Zenodo with persistent DOIs. A public version of the code repository will also be maintained on GitHub [URL to be added after acceptance]. WWLLN lightning data were obtained upon request from the World Wide Lightning Location Network (https://wwlln.net) and are not publicly available.

**Competing interests**

The authors declare no competing interests.

**Consent for publication**

Not applicable.

**Ethics approval and consent to participate**

Not applicable

# References

1. Amador JA, Arce-Fernández D (2022) WWLLN hot and cold-spots of lightning activity and their relation to climate in an extended Central America region 2012–2020. Atmosphere (Basel) 13:76. https://doi.org/10.3390/atmos13010076

2. Baker B, Baker MB, Jayaratne ER, Latham J, Saunders CPR (1987) The Influence of Diffusional Growth Rates On the Charge Transfer Accompanying Rebounding Collisions Between Ice Crystals and Soft Hailstones. Quarterly Journal of the Royal Meteorological Society 113:1193–1215. https://doi.org/10.1002/qj.49711347807
3. Baker MB, Dash JG (1994) Mechanism of charge transfer between colliding ice particles in thunderstorms. Journal of Geophysical Research: Atmospheres 99:10621–10626. https://doi.org/https://doi.org/10.1029/93JD01633
4. Beucler T, Gentine P, Yuval J, Gupta A, Peng L, Lin J, Yu S, Rasp S, Ahmed F, O'Gorman PA, Neelin JD, Lutsko NJ, Pritchard M (2024) Climate-invariant machine learning. Sci Adv 10. https://doi.org/10.1126/sciadv.adj7250
5. Bieniek PA, Bhatt US, York A, Walsh JE, Lader R, Strader H, Ziel R, Jandt RR, Thoman RL (2020) Lightning variability in dynamically downscaled simulations of Alaska's present and future summer climate. J Appl Meteorol Climatol 59:1139–1152. https://doi.org/10.1175/JAMC-D-19-0209.1
6. Brienen RJW, Phillips OL, Feldpausch TR, Gloor E, Baker TR, Lloyd J, Lopez-Gonzalez G, Monteagudo-Mendoza A, Malhi Y, Lewis SL, Vásquez Martinez R, Alexiades M, Álvarez Dávila E, Alvarez-Loayza P, Andrade A, Aragão LEOC, Araujo-Murakami A, Arets EJMM, Arroyo L, Aymard C. GA, Bánki OS, Baraloto C, Barroso J, Bonal D, Boot RGA, Camargo JLC, Castilho C V., Chama V, Chao KJ, Chave J, Comiskey JA, Cornejo Valverde F, da Costa L, de Oliveira EA, Di Fiore A, Erwin TL, Fauset S, Forsthofer M, Galbraith DR, Grahame ES, Groot N, Hérault B, Higuchi N, Honorio Coronado EN, Keeling H, Killeen TJ, Laurance WF, Laurance S, Licona J, Magnussen WE, Marimon BS, Marimon-Junior BH, Mendoza C, Neill DA, Nogueira EM, Núñez P, Pallqui Camacho NC, Parada A, Pardo-Molina G, Peacock J, Peña-Claros M, Pickavance GC, Pitman NCA, Poorter L, Prieto A, Quesada CA, Ramírez F, Ramírez-Angulo H, Restrepo Z, Roopsind A, Rudas A, Salomão RP, Schwarz M, Silva N, Silva-Espejo JE, Silveira M, Stropp J, Talbot J, ter Steege H, Teran-Aguilar J, Terborgh J, Thomas-Caesar R, Toledo M, Torello-Raventos M, Umetsu RK, van der Heijden GMF, van der Hout P, Guimarães Vieira IC, Vieira SA, Vilanova E, Vos VA, Zagt RJ (2015) Long-term decline of the Amazon carbon sink. Nature 519:344–348. https://doi.org/10.1038/nature14283
7. Cecil DJ, Buechler DE, Blakeslee RJ (2014) Gridded lightning climatology from TRMM-LIS and OTD: dataset description. Atmos Res 135–136:404–414. https://doi.org/10.1016/j.atmosres.2012.06.028
8. Chakraborty R, Chakraborty A, Basha G, Ratnam MV (2021) Lightning occurrences and intensity over the Indian region: long-term trends and future projections. Atmos Chem Phys 21:11161–11177
9. Chen Y, Romps DM, Seeley JT, Veraverbeke S, Riley WJ, Mekonnen ZA, Randerson JT (2021) Future increases in Arctic lightning and fire risk for permafrost carbon. Nat Clim Chang 11:404–410. https://doi.org/10.1038/s41558-021-01011-y
10. Cochrane MA, Laurance WF (2008) Synergisms among fire, land use, and climate change in the Amazon. AMBIO: A Journal of the Human Environment 37:522–527. https://doi.org/10.1579/0044-7447-37.7.522

11. Del Genio AD, Yao M, Jonas J (2007) Will moist convection be stronger in a warmer climate? Geophys Res Lett 34. https://doi.org/10.1029/2007GL030525
12. dos Santos APP, Pinto JO, dos Santos SRQ, de Lima FJL, de Souza EB, de Morais AAR, Ávila EE, Pedernera A (2017) Climatic projections of lightning in southeastern brazil using cmip5 models in rcp's scenarios 4.5 and 8.5. Am J Clim Change 6:539
13. Döscher R, Acosta M, Alessandri A, Anthoni P, Arsouze T, Bergman T, Bernardello R, Boussetta S, Caron L-P, Carver G, Castrillo M, Catalano F, Cvijanovic I, Davini P, Dekker E, Doblas-Reyes FJ, Docquier D, Echevarria P, Fladrich U, Fuentes-Franco R, Gröger M, v. Hardenberg J, Hieronymus J, Karami MP, Keskinen J-P, Koenigk T, Makkonen R, Massonnet F, Ménégoz M, Miller PA, Moreno-Chamarro E, Nieradzik L, van Noije T, Nolan P, O'Donnell D, Ollinaho P, van den Oord G, Ortega P, Prims OT, Ramos A, Reerink T, Rousset C, Ruprich-Robert Y, Le Sager P, Schmith T, Schrödner R, Serva F, Sicardi V, Sloth Madsen M, Smith B, Tian T, Tourigny E, Uotila P, Vancoppenolle M, Wang S, Wårlind D, Willén U, Wyser K, Yang S, Yepes-Arbós X, Zhang Q (2022) The EC-Earth3 Earth system model for the Coupled Model Intercomparison Project 6. Geosci Model Dev 15:2973–3020. https://doi.org/10.5194/gmd-15-2973-2022
14. Dowden RL, Brundell JB, Rodger CJ (2002) VLF lightning location by time of group arrival (TOGA) at multiple sites. J Atmos Sol Terr Phys 64:817–830. https://doi.org/https://doi.org/10.1016/S1364-6826(02)00085-8
15. Feddersen H, Navarra A, Ward NM (1999) Reduction of model systematic error by statistical correction for dynamical seasonal predictions
16. Finney DL, Doherty RM, Wild O, Huntrieser H, Pumphrey HC, Blyth AM (2014) Using cloud ice flux to parametrise large-scale lightning. Atmos Chem Phys 14:12665–12682. https://doi.org/10.5194/acp-14-12665-2014
17. Finney DL, Doherty RM, Wild O, Stevenson DS, MacKenzie IA, Blyth AM (2018) A projected decrease in lightning under climate change. Nat Clim Chang 8:210–213
18. Finney DL, Marsham JH, Wilkinson JM, Field PR, Blyth AM, Jackson LS, Kendon EJ, Tucker SO, Stratton RA (2020) African lightning and its relation to rainfall and climate change in a convection-permitting model. Geophys Res Lett 47. https://doi.org/10.1029/2020GL088163
19. Gan MA, Kousky VE, Ropelewski CF (2004) The South America Monsoon Circulation and Its Relationship to Rainfall over West-Central Brazil
20. Gora EM, Burchfield JC, Muller-Landau HC, Bitzer PM, Yanoviak SP (2020) Pantropical geography of lightning-caused disturbance and its implications for tropical forests. Glob Chang Biol 26:5017–5026. https://doi.org/10.1111/gcb.15227
21. Hersbach H, Bell B, Berrisford P, Biavati G, Horányi A, Muñoz Sabater J, Nicolas J, Peubey C, Radu R, Rozum I, Schepers D, Simmons A, Soci C, Dee D, Thépaut J-N (2023a) ERA5 monthly averaged data on single levels from 1940 to present
22. Hersbach H, Bell B, Berrisford P, Biavati G, Horányi A, Muñoz Sabater J, Nicolas J, Peubey C, Radu R, Rozum I, Schepers D, Simmons A, Soci C, Dee D, Thépaut J-N (2023b) ERA5 monthly averaged data

on pressure levels from 1940 to present

23. Holle RL (2016) A Summary of Recent National-Scale Lightning Fatality Studies. Weather, Climate, and Society 8:35–42. https://doi.org/10.1175/WCAS-D-15-0032.1
24. Holzworth RH, Brundell JB, McCarthy MP, Jacobson AR, Rodger CJ, Anderson TS (2021) Lightning in the Arctic. Geophys Res Lett 48. https://doi.org/10.1029/2020GL091366
25. Hutchins ML, Holzworth RH, Brundell JB, Rodger CJ (2012) Relative detection efficiency of the World Wide Lightning Location Network. Radio Sci 47. https://doi.org/10.1029/2012RS005049
26. Jiang H, Liao H (2013) Projected changes in NOx emissions from lightning as a result of 2000–2050 climate change. Atmospheric and Oceanic Science Letters 6
27. Johnson MO, Galbraith D, Gloor M, De Deurwaerder H, Guimberteau M, Rammig A, Thonicke K, Verbeeck H, von Randow C, Monteagudo A, Phillips OL, Brienen RJW, Feldpausch TR, Lopez Gonzalez G, Fauset S, Quesada CA, Christoffersen B, Ciais P, Sampaio G, Kruijt B, Meir P, Moorcroft P, Zhang K, Alvarez-Davila E, Alves de Oliveira A, Amaral I, Andrade A, Aragao LEOC, Araujo-Murakami A, Arets EJMM, Arroyo L, Aymard GA, Baraloto C, Barroso J, Bonal D, Boot R, Camargo J, Chave J, Cogollo A, Cornejo Valverde F, Lola da Costa AC, Di Fiore A, Ferreira L, Higuchi N, Honorio EN, Killeen TJ, Laurance SG, Laurance WF, Licona J, Lovejoy T, Malhi Y, Marimon B, Marimon BH, Matos DCL, Mendoza C, Neill DA, Pardo G, Peña-Claros M, Pitman NCA, Poorter L, Prieto A, Ramirez-Angulo H, Roopsind A, Rudas A, Salomao RP, Silveira M, Stropp J, ter Steege H, Terborgh J, Thomas R, Toledo M, Torres-Lezama A, van der Heijden GMF, Vasquez R, Guimarães Vieira IC, Vilanova E, Vos VA, Baker TR (2016) Variation in stem mortality rates determines patterns of above-ground biomass in amazonian forests: implications for dynamic global vegetation models. Glob Chang Biol 22:3996–4013. https://doi.org/10.1111/gcb.13315
28. Kahraman A, Kendon EJ, Fowler HJ, Wilkinson JM (2022) Contrasting future lightning stories across Europe. Environmental Research Letters 17. https://doi.org/10.1088/1748-9326/ac9b78
29. Koshak WJ, Cummins KL, Buechler DE, Vant-Hull B, Blakeslee RJ, Williams ER, Peterson HS (2015) Variability of CONUS lightning in 2003–12 and associated impacts. J Appl Meteorol Climatol 54:15–41. https://doi.org/10.1175/JAMC-D-14-0072.1
30. Krause A, Kloster S, Wilkenskjeld S, Paeth H (2014) The sensitivity of global wildfires to simulated past, present, and future lightning frequency. J Geophys Res Biogeosci 119:312–322. https://doi.org/10.1002/2013JG002502
31. Marengo JA, Espinoza J-C, Fu R, Jimenez Muñoz JC, Alves LM, Da Rocha HR, Schöngart J (2024) Long-term variability, extremes and changes in temperature and hydrometeorology in the Amazon region: A review. Acta Amazon 54. https://doi.org/10.1590/1809-4392202200980
32. Michalon N, Nassif A, Saouri T, Royer JF, Pontikis CA (1999) Contribution to the climatological study of lightning. Geophys Res Lett 26:3097–3100. https://doi.org/10.1029/1999GL010837
33. Molina MJ, Gagne DJ, Prein AF (2021) A Benchmark to Test Generalization Capabilities of Deep Learning Methods to Classify Severe Convective Storms in a Changing Climate. Earth and Space Science 8. https://doi.org/10.1029/2020EA001490

34. Naccarato KP, dos Santos APP, de Lima FJL (2022) Incidence of lightning strikes to power transmission lines in the south of Brazil: current and future climate. In: INTERNATIONAL CONFERENCE ON LIGHTNING PROTECTION, 2022. Proceedings of the International Conference on Lightning Protection. IEEE, pp 311–314
35. O'Neill BC, Tebaldi C, Van Vuuren DP, Eyring V, Friedlingstein P, Hurtt G, Knutti R, Kriegler E, Lamarque J-F, Lowe J (2016) The scenario model intercomparison project (ScenarioMIP) for CMIP6. Geosci Model Dev 9:3461–3482
36. Paulucci TB, França GB, Libonati R, Ramos AM (2019) Long-term spatial–temporal characterization of cloud-to-ground lightning in the metropolitan region of Rio de Janeiro. Pure Appl Geophys 176:5161–5175. https://doi.org/10.1007/s00024-019-02216-1
37. Pérez-Invernón FJ, Gordillo-Vázquez FJ, Huntrieser H, Jöckel P (2023) Variation of lightning-ignited wildfire patterns under climate change. Nat Commun 14:739. https://doi.org/10.1038/s41467-023-36500-5
38. Pivello VR (2011) The use of fire in the Cerrado and Amazonian Rainforests of Brazil: past and present. Fire Ecology 7:24–39. https://doi.org/10.4996/fireecology.0701024
39. Price C, Rind D (1994) Possible implications of global climate change on global lightning distributions and frequencies. Journal of Geophysical Research: Atmospheres 99:10823–10831. https://doi.org/10.1029/94JD00019
40. Price C, Rind D (1990) The effect of global warming on lightning frequencies. In: CONFERENCE ON SEVERE LOCAL STORMS, 16., 1990, Kananaskis Park, Canadá. Proceedings of the 16th Conference on Severe Local Storms. American Meteorological Society
41. Rao VB, Hada K (1990) Characteristics of rainfall over Brazil: Annual variations and connections with the Southern Oscillation. Theor Appl Climatol 42:81–91. https://doi.org/10.1007/BF00868215
42. Reboita MS, Willian de Souza Ferreira G, Gabriel Martins Ribeiro J, Ali S (2024) Assessment of precipitation and near-surface temperature simulation by CMIP6 models in South America. Environmental Research: Climate 3:025011. https://doi.org/10.1088/2752-5295/ad3fdb
43. Rehbein A, Ambrizzi T, Prein AF (2026) South American Mesoscale Convective Systems: Present and Future Climates. Journal of Geophysical Research: Atmospheres 131. https://doi.org/10.1029/2025JD045438
44. Ribeiro BZ, Seluchi ME (2019) A climatology of quasi-linear convective systems and associated synoptic-scale environments in southern Brazil. International Journal of Climatology 39:857–877. https://doi.org/10.1002/joc.5847
45. Romps DM (2019) Evaluating the future of lightning in cloud-resolving models. Geophys Res Lett 46:14863–14871. https://doi.org/10.1029/2019GL085748
46. Romps DM, Seeley JT, Vollaro D, Molinari J (2014) Projected increase in lightning strikes in the United States due to global warming. Science (1979) 346:851–854. https://doi.org/10.1126/science.1259100

47. Sinha A, Toumi R (1997) Tropospheric ozone, lightning, and climate change. Journal of Geophysical Research: Atmospheres 102:10667–10672. https://doi.org/10.1029/96JD03710
48. Slik JWF, Paoli G, McGuire K, Amaral I, Barroso J, Bastian M, Blanc L, Bongers F, Boundja P, Clark C, Collins M, Dauby G, Ding Y, Doucet J, Eler E, Ferreira L, Forshed O, Fredriksson G, Gillet J, Harris D, Leal M, Laumonier Y, Malhi Y, Mansor A, Martin E, Miyamoto K, Araujo-Murakami A, Nagamasu H, Nilus R, Nurtjahya E, Oliveira Á, Onrizal O, Parada-Gutierrez A, Permana A, Poorter L, Poulsen J, Ramirez-Angulo H, Reitsma J, Rovero F, Rozak A, Sheil D, Silva-Espejo J, Silveira M, Spironelo W, ter Steege H, Stevart T, Navarro-Aguilar GE, Sunderland T, Suzuki E, Tang J, Theilade I, van der Heijden G, van Valkenburg J, Van Do T, Vilanova E, Vos V, Wich S, Wöll H, Yoneda T, Zang R, Zhang M, Zweifel N (2013) Large trees drive forest aboveground biomass variation in moist lowland forests across the tropics. Global Ecology and Biogeography 22:1261–1271. https://doi.org/10.1111/geb.12092
49. Whaley C, Etten-Bohm M, Schumacher C, Akingunola A, Arora V, Cole J, Lazare M, Plummer D, von Salzen K, Winter B (2024) A new lightning scheme in the Canadian Atmospheric Model (CanAM5.1): implementation, evaluation, and projections of lightning and fire in future climates. Geosci Model Dev 17:7141–7155. https://doi.org/10.5194/gmd-17-7141-2024
50. Wilks DS (2011) Statistical methods in the atmospheric sciences. Academic press
51. Wood AW, Maurer EP, Kumar A, Lettenmaier DP (2002) Long-range experimental hydrologic forecasting for the eastern United States. Journal of Geophysical Research: Atmospheres 107:ACL 6-1-ACL 6-15. https://doi.org/10.1029/2001JD000659

# Figures

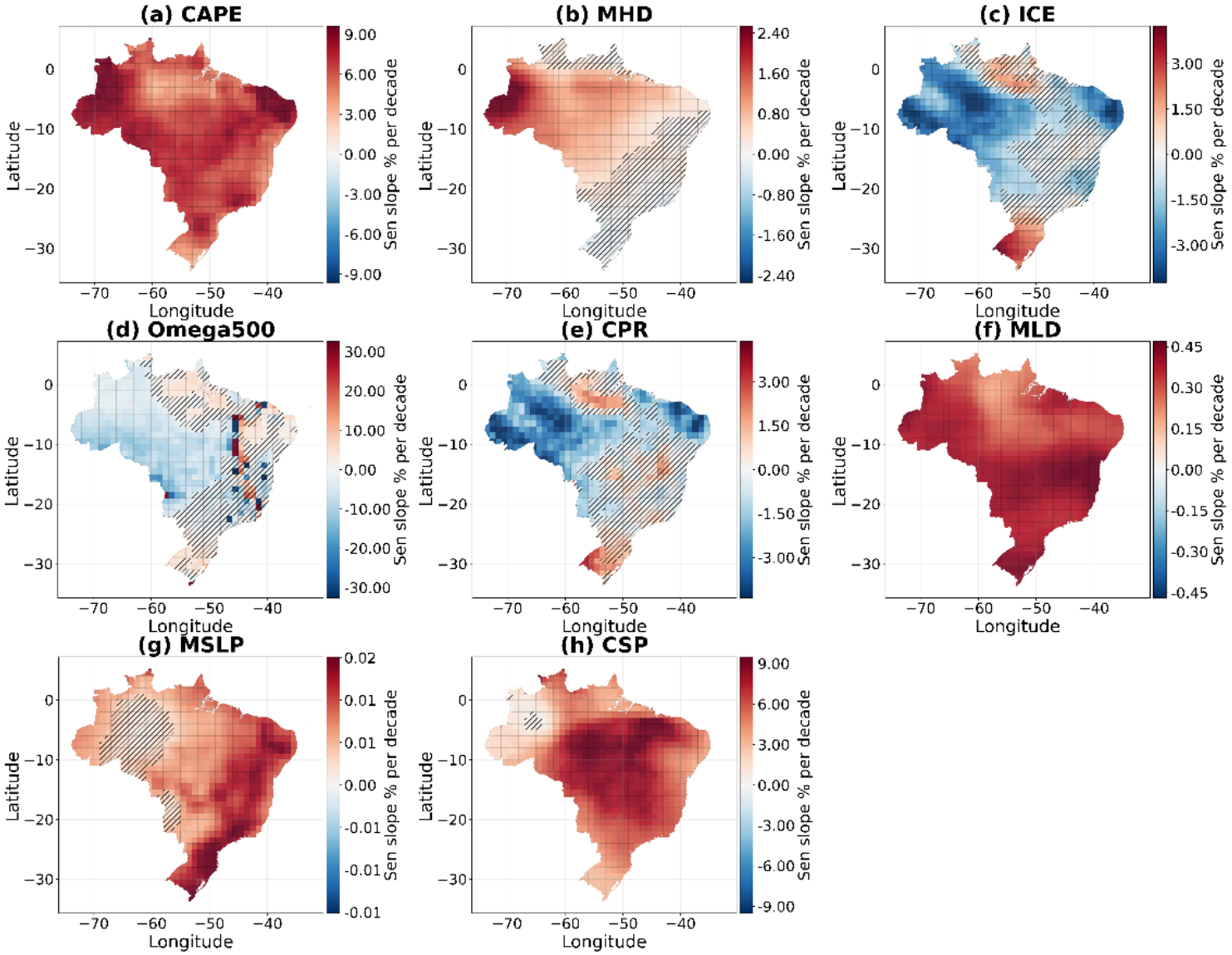



**Figure 1**

Decadal percentage trend of annual mean atmospheric variables under the SSP585 scenario. Eight atmospheric variables from the bias-corrected EC-EARTH3-VEG model projections (2015–2100) are shown: (a) Convective Available Potential Energy (CAPE), (b) Mid-Level Humidity Deficit (MHD), (c) Total Column Ice (ICE), (d) Vertical Velocity at 500 hPa (Omega500), (e) Convective Precipitation Rate (CPR), (f) Mixed-Phase Layer Depth (MPD), (g) Mean Sea Level Pressure (MSLP), and (h) Conditional Stability Proxy (CSP). Bias correction was performed through mean and variance adjustment relative to ERA5 reanalysis observations (reference period: 2013-2025). Trends were calculated using Sen's slope and are expressed as percentage change per decade relative to the mean climatology of each grid cell. Hatched areas (///) indicate regions where the Mann-Kendall test yielded a p-value ≥ 0.05, representing statistically non-significant trends.

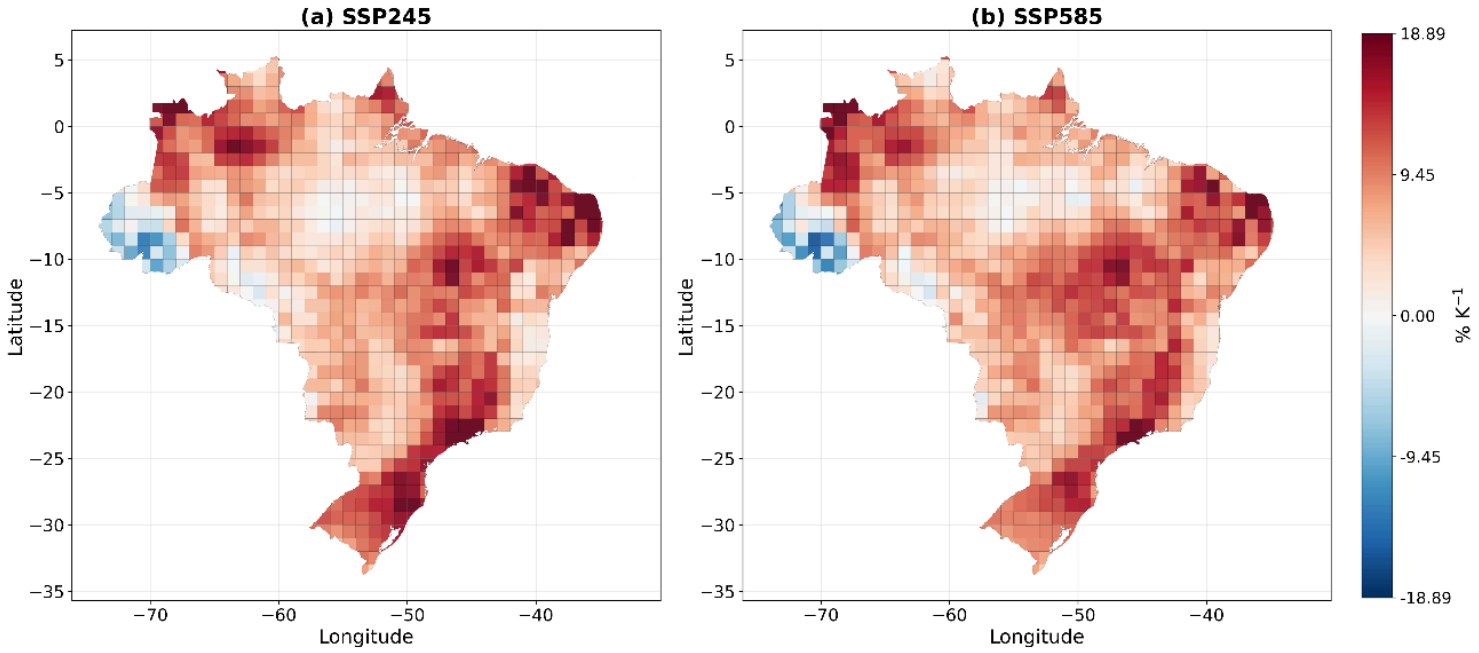



**Figure 2**

Spatial distribution of fractional changes in lightning density (% $K^{-1}$) for 2071–2100 relative to the present-day climate (2013–2025), under the (a) SSP2-4.5 and (b) SSP5-8.5 scenarios, normalized by the mean global temperature change from EC-EARTH3-VEG. Lightning projections were derived from multiple linear regression models trained with the ERA5 reanalysis (2013–2022), using CAPE (Convective Available Potential Energy), ICE (Column-Integrated Atmospheric Ice), and MSLP (Mean Sea-Level Pressure) as predictors. The color scale ranges from reductions (blue) to increases (red) in electrical activity. The metric represents the sensitivity of lightning density per kelvin of global warming.

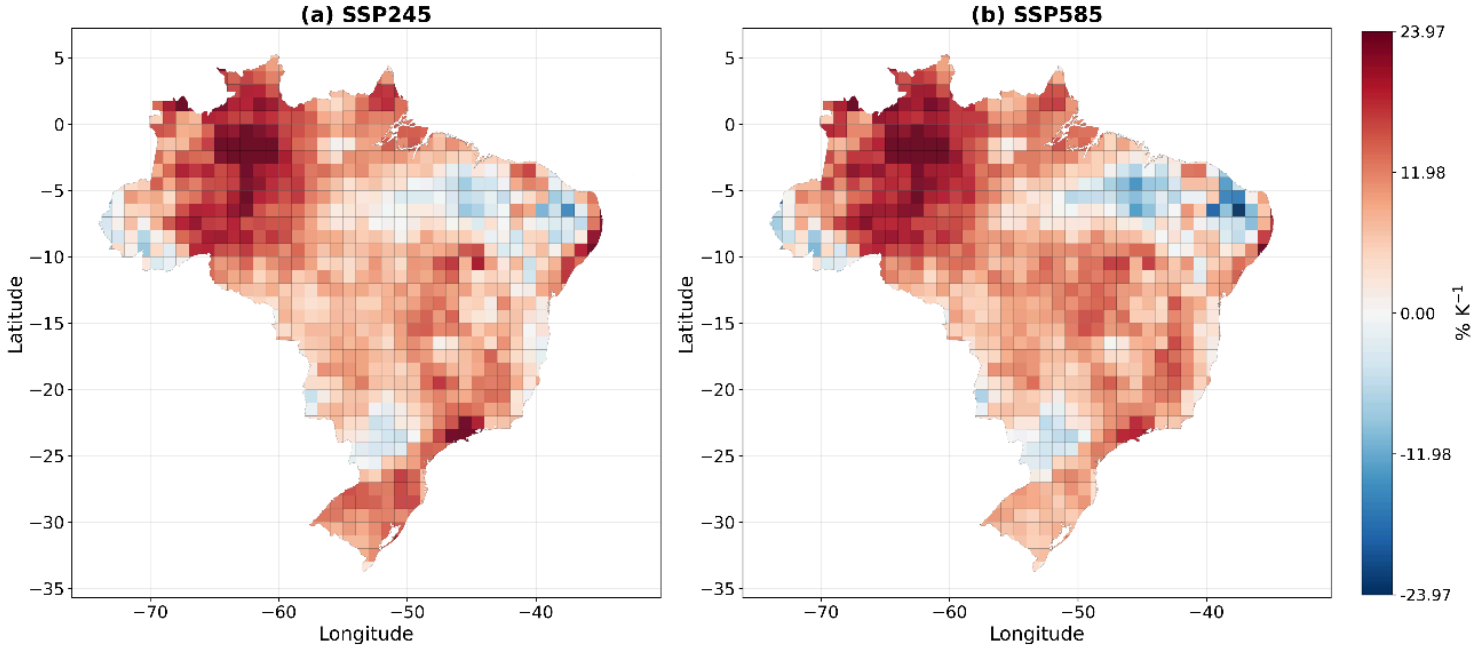



**Figure 3**

Spatial distribution of fractional changes in lightning density (% $K^{-1}$) for 2071–2100 relative to the present-day climate (2013-2025), under the (a) SSP2-4.5 and (b) SSP5-8.5 scenarios, normalized by the mean global temperature change from EC-EARTH3-VEG. Lightning projections were derived from multiple linear regression models trained with the ERA5 reanalysis (2013-2022), using CAPE (Convective Available Potential Energy), CPR (Convective Precipitation Rate), MPD (Mixed-Phase Layer Depth), and MSLP (Mean Sea-Level Pressure) as predictors. The color scale ranges from reductions (blue) to increases (red) in electrical activity. The metric represents the sensitivity of lightning density per kelvin of global warming.

## Supplementary Files

This is a list of supplementary files associated with this preprint. Click to download.

- SupplementaryMaterial.docx
- SupplementaryTable2.xlsx